Numerical Study on Hydrodynamic Interaction between Two Tankers in Shallow Water Based on High-Order Panel Method

Hua-Fu Xu [a,c], Lu Zou [a,b*], Zao-Jian Zou [a,b], Zhi-Ming Yuan [d]

[a]School of Naval Architecture, Ocean and Civil Engineering, Shanghai Jiao Tong University, Shanghai 200240, China
[b]Collaborative Innovation Center for Advanced Ship and Deep-Sea Exploration, Shanghai Jiao Tong University, Shanghai 200240, China
[*] E-mail: luzou@sjtu.edu.cn
[c]Development and Reform Commission of Beihai, Beihai 536000, Guangxi, China
[d]Department of Naval Architecture, Ocean and Marine Engineering, University of Strathclyde, Glasgow, UK

ABSTRACT

A three-dimensional high-order panel method based on Non-Uniform Rational B-Spline (NURBS) for predicting the ship-ship hydrodynamic interaction during meeting and overtaking in shallow water is developed. The NURBS surface is used to precisely represent the hull geometry. The velocity potential on the body surface is described by B-spline after the source density distribution on the boundary surface is determined. A collocation approach is applied to the boundary integral equation discretization, and the velocity potential is being solved at each time step. Under the low-speed assumption, the effect of free surface elevation is neglected in the numerical calculation, and the infinite image method is used to deal with the finite water depth effect. Two tankers in model tests are investigated, and the predicted hydrodynamic interaction forces and moments are compared with experimental measurements to clarify the validity of the proposed numerical method. Calculations are then conducted for different water depths, lateral ship-ship distances and ship speeds, and the detailed results are discussed to demonstrate the effects of these factors.

Key words: High-order panel method; NURBS; ship-ship hydrodynamic interaction; shallow water; meeting; overtaking

1. Introduction

Ship-to-ship hydrodynamic interactions involving significant hydrodynamic forces and moments will occur when two ships are moving in close proximity. Particular cases of special interest are the unsteady-state situations such as two ships moving side by side during replenishment or lightering operations, and two ships meeting or overtaking in waterways. In these cases, hydrodynamic interaction forces and moments on the ships may lead to accidents such as collision, and this could be more dangerous in shallow waterways, where the shallow-water effect is remarkable.

Many previous studies on this subject were based on the experimental method since it typically produced reliable and realistic results. An early effort was made by Remery [1] who tested the interaction effects of a passing ship on a moored tanker in shallow water. Vantorre et al. [2] carried out a series of experimental study on ship-ship hydrodynamic interaction in shallow water involving various ship types. The influences of many important factors, such as the ratios of ship speeds, ship lengths, and ship drafts, the lateral distance between ships, the water depth and the under keel clearance, were investigated. Based on regression analysis of the experimental data, empirical formulae for predicting the peak values of ship-ship hydrodynamic interaction were proposed. A set of more extensive captive model tests in shallow water were conducted by Lataire et al. [3] for evaluating the influences of water depth, ship draft, drift angle, speed and relative distance in ship-ship lightering operations of two tankers. Later, the model tests were served as benchmark test cases in the 2nd International Conference on Ship Manoeuvring in Shallow and Confined Water (MASHCON): Ship-to-Ship Interaction (2011) [4] and were widely used in several benchmark studies for validating the capability of numerical methods.

Theoretical study of ship-ship hydrodynamic interaction was traditionally based on the slender-body

theory. Tuck and Newman [5] extended the slender-body theory to predict the hydrodynamic lateral force and yaw moment acting on each of two ships while they were moving along parallel paths in both deep and shallow waters. A similar approach was used by Yeung [6] to study the unsteady hydrodynamic interaction of two slender ships moving in shallow water. This study was extended by Wang [7] who investigated the irrotational flow passing two slender bodies of revolution at angles of yaw, translating in parallel paths in very close proximity. In all the studies mentioned above, the effects of free surface elevation were ignored under the assumption of low moving speeds.

During the last decades, many numerical studies on ship-ship hydrodynamic interaction have been carried out based on the three-dimensional (3D) Rankine source panel method proposed by Hess and Smith [8]. Korsmeyer et al. [9] studied the ship-ship hydrodynamic interaction between two slender ships and the bank effects in a rectangular canal by using a rectangular Green function derived by Newman [10] coupled with the Rankine source panel method. The canal with sloping banks was also considered. Zhang and Wu [11] studied the hydrodynamic interactions between two similar Wigley ships under meeting and passing conditions in narrow waterway by using panel method. Yasukawa et al. [12] investigated the ship-bank and ship-ship hydrodynamic interaction in encountering and overtaking conditions for actual ships such as ferry, container ship and tanker by using a 3D panel method with the assumption of rigid free-surface. The qualitative tendency of the interaction forces was captured appropriately, but the quantitative accuracy is insufficient. Sutulo et al. [13, 14] developed a potential code for calculating ship-ship hydrodynamic interaction also by using the classic Hess and Smith panel method and the code was validated against experimental data obtained in deep and shallow water towing tanks for two identical S175 container vessels. Zhou et al. further extended the code to the restricted water cases based on the double-body model and panel method for calculating ship-ship hydrodynamic interaction, a so-called “moving-patch” method [15, 16], and a paving algorithm [17] for better mesh generation was introduced for simulating bottom of arbitrary geometry instead of flat. Yuan et al. [18, 19] developed a boundary element program based on 3D Rankine source method, and the hydrodynamic interactions of two ships overtaking in shallow water (with the minimum water depth to draft ratio 2.0) or during a lightering operation at different forward speeds were investigated and satisfactory results were obtained. It should be noted that the Rankine source potential method using constant panel method can only generate flat panels and is not able to describe the hull geometry smoothly, thus the high-order panel method may be a better option. Zhang et al. [20] developed a numerical computation method based on B-splines for predicting the hydrodynamic interaction between two Wigley ships. The B-spline functions were employed to approximate both the ship geometry and the unknown velocity potential. Lately, Xu et al. [21-24] developed a high-order panel method based on Non-Uniform Rational B-Spline (NURBS) and predicted the ship-ship hydrodynamic interaction forces on two Wigley hulls including the shallow water effects and bank effects.

In recent years, there were also many researches on ship-ship hydrodynamic interaction by using viscous method, typically, the Reynolds Averaged Navier-Stokes (RANS)-based method. Chen et al. [25] calculated the unsteady ship-ship hydrodynamic interaction in shallow water and restricted navigation channels by using RANS method in conjunction with a chimera domain decomposition approach. Zhang and Zou [26] carried out a numerical study on the hydrodynamic interaction between ships meeting and overtaking in restricted waters by solving unsteady RANS equations. Particularly as mentioned before, several validation studies concerning ship-ship interaction during lightering operation in shallow water [27-30] have been performed making use of the benchmark test cases at the 2nd MASHCON conference [4] and applying different RANS models or meshing techniques. Besides, Wang and Zou [31] carried out a numerical study on the hydrodynamic interaction between a berthed ship and a passing ship entering and leaving a single-way lock by solving the unsteady RANS equations. The influences of some factors, such as ship speed, water depth, transverse and longitudinal positions of the berthed ship were investigated. Recently, Kok et al. [32] performed similar investigations on the hydrodynamic interactions between berthed and passing ships in both model and full scale using unsteady RANS method. The numerical model showed reasonable agreement to the experiments by Remery [1] for model-scale computations and the scale effects were discussed subsequently.

Among the theoretical and numerical methods for predicting ship-ship hydrodynamic interaction in restricted waters, slender-body theory can provide a quick and real-time prediction, while its prediction accuracy is questionable, especially for the modern full-formed ships. In principle, the viscous methods can

provide more accurate prediction; however, they are time-consuming and not suitable for practical and real-time application. By contrast, the potential flow method is a good compromise between accuracy and efficiency, since it can provide a more practical and relatively effective prediction of the hydrodynamic interactions. The potential flow methods primarily are based on constant panel method which is not able to represent the body surface in a precise way. Due to this limitation, most of the previous studies dealt with mathematical or relatively simple ship hull forms for ship-ship interaction problems and only moderate water depth was considered.

The high-order panel method can provide a more precise description of the body geometry and can be used to represent the source density or velocity potential distribution for potential flow problem, guaranteeing the continuity of higher order derivatives of velocity potential on the body surface. In previous work, the authors have developed a high-order panel method based on NURBS [21] to investigate the ship-ship interaction problems in shallow waters [22, 23] or in canals [24], and only the mathematical ship hull (i.e., Wigley) was investigated. In the present paper, this method is extended to calculate the ship-to-ship interaction between two real ships during meeting and overtaking in shallow waters, and more comprehensive computations are conducted. A NURBS surface is used to precisely represent the body geometry. The velocity potential distribution on the body surface is described by B-spline after the source density distribution on the body surface is determined. The collocation method is adopted with the collocation points distributed on the vertices of NURBS surface, and the singularity sources are distributed on the Gaussian points of each panel on the NURBS surface. Under the assumption of low ship speed, the effect of free surface elevation is ignored, and the infinite image method is used to deal with the finite water depth effect. Calculations are carried out for different water depths, lateral ship-ship distances between broadsides and ship speeds to analyze the influences of these factors.

2. Mathematical formulation

Two ships moving along parallel courses in proximity of each other are considered, one ship (Ship 1) navigates with a constant speed U_1, and the other ship (Ship 2) navigates with a constant speed U_2, as shown in Fig. 1. The coordinate systems o-xyz fixed in the space and o_i-$x_iy_iz_i$ fixed to Ship i (i=1, 2) are adopted, where the x_i-axis is pointing from ship stern to the bow, y_i-axis to starboard side and z_i-axis vertically downward; the o_i-x_iy_i plane coincides with the undisturbed free surface (z = 0). As indicated in Fig.1, the axis directions of the coordinate system on Ship 1 are identical to those of o-xyz. The water depth is assumed to be constant and expressed by h. The longitudinal and transverse distances between the ships are denoted by ST and Sp, and the lateral distance between the ships' broadsides are defined as y_{bb}.

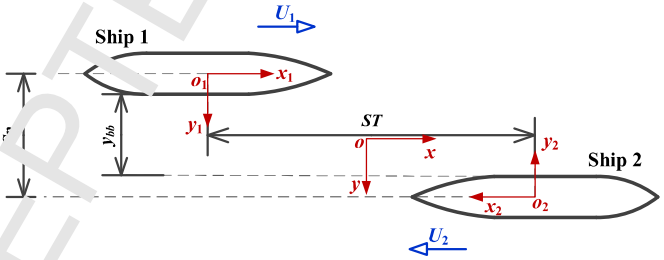

(a) Top view

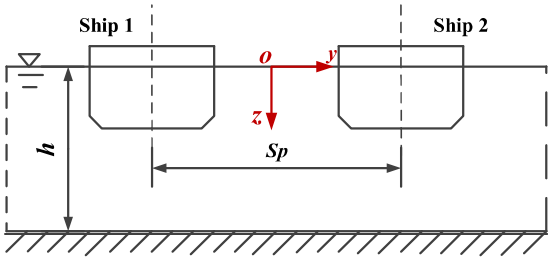

(b) Back view

Fig. 1. Sketch of ship-to-ship interaction

It is assumed that 1) The fluid is inviscid and the flow is irrotational; 2) The ship speeds are very small, so that the effects of free-surface elevation can be ignored. Furthermore, the shedding of vortices due to the viscous effect and flow separation is neglected. The neglect of free-surface effects and shed vortices removes all the memory effects and allows the solution to be stepped through time as a series of independent hydrodynamic calculations [9].

The perturbation velocity potential representing the flow is defined as $\phi(t,x,y,z)$, it satisfies the Laplace equation in the fluid domain and the following boundary conditions:

$$\frac{\partial \phi}{\partial n^{(1)}} = U_1 n_1^{(1)}, \text{ on } S_1 \tag{1}$$

$$\frac{\partial \phi}{\partial n^{(2)}} = U_2 n_1^{(2)}, \text{ on } S_2 \tag{2}$$

$$\frac{\partial \phi}{\partial z} = 0, \text{ on } z = 0 \tag{3}$$

$$\frac{\partial \phi}{\partial z} = 0, \text{ on } z = h \tag{4}$$

where $\overrightarrow{n^{(i)}} = \left(n_1^{(i)}, n_2^{(i)}, n_3^{(i)}\right)$ and S_i denote the outward normal vector and the hull surface of Ship i, respectively.

The velocity potential ϕ is expressed by source distribution on the hull surfaces as follows:

$$\phi(t,P) = \iint_{S_1} \sigma^{(1)}(t,Q)G(P;Q)dS + \iint_{S_2} \sigma^{(2)}(t,Q)G(P;Q)dS \tag{5}$$

where $\sigma^{(i)}$ denotes the strength of source distributed on the hull surface of Ship i. $P(x, y, z)$ is a field point and $Q(\varsigma, \eta, \zeta)$ is a singular point on the surface S which consists of the wetted surfaces S_1 and S_2.

The Green function takes the following form:

$$G(x,y,z;\varsigma,\eta,\zeta) = \sum_{a=-\infty}^{\infty}\left(\frac{1}{r_a} + \frac{1}{\overline{r}_a}\right) \tag{6}$$

where: $r_a = \sqrt{(x-\varsigma)^2 + (y-\eta)^2 + (z-\zeta+2an)^2}$ and $\overline{r}_a = \sqrt{(x-\varsigma)^2 + (y-\eta)^2 + (z+\zeta+2ah)^2}$, a is an integer.

With application of this Green function of infinite mirror-image, the boundary conditions (3) and (4) on the undisturbed free surface and the sea bottom are satisfied automatically; while by satisfying the boundary conditions (1) and (2) on the hull surfaces, it follows the following Fredholm integral equation of second kind:

$$2\pi\sigma(t,P) + \iint_S \sigma(t,Q)\frac{\partial G(P,Q)}{\partial n(P)}dS(Q) = \begin{cases} U_1 n_1^{(1)}, & P \in S_1 \\ U_2 n_1^{(2)}, & P \in S_2 \end{cases} \tag{7}$$

Once Eq. (7) is solved, the disturbance velocity potential and disturbance velocity can be expressed through the density σ by Eq. (5) and Eq. (8):

$$\overrightarrow{V}(t,P) = \iint_S \sigma(t,Q)\nabla_P G(P;Q)dS(Q) \tag{8}$$

The pressure distribution on Ship i is determined from the unsteady Bernoulli equation in the following form:

$$p = -\rho\left(\frac{\partial \phi}{\partial t} - U_i \phi_x + \frac{1}{2}\nabla\phi\cdot\nabla\phi\right) \tag{9}$$

Then, the hydrodynamic force $\overrightarrow{F_i}$ and moment $\overrightarrow{N_i}$ acting on Ship i can be determined:

$$\vec{F}_i = -\iint_{S_i} p\vec{n}dS \ , \ \vec{M}_i = -\iint_{S_i} p(\vec{r}_i \times \vec{n})dS \tag{10}$$

where $\vec{r}_i = (x_i, y_i, z_i)$.

3. Solution procedure of the panel method based on NURBS

In present study, not only the body geometry, but also the source density is described by NURBS. The expressions of an arbitrary point P and the distributed source density σ on the body surface at a given moment take the forms:

$$P(u,v) = \frac{\sum_{i=0}^{m}\sum_{j=0}^{n} w_{ij} D_{ij} N_{i,k}(u) N_{j,l}(v)}{\sum_{i=0}^{m}\sum_{j=0}^{n} w_{ij} N_{i,k}(u) N_{j,l}(v)} \tag{11}$$

$$\sigma(u,v) = \frac{\sum_{i=0}^{m}\sum_{j=0}^{n} w_{ij} S_{ij} N_{i,k}(u) N_{j,l}(v)}{\sum_{i=0}^{m}\sum_{j=0}^{n} w_{ij} N_{i,k}(u) N_{j,l}(v)} \tag{12}$$

where u, v are the parameters representing two directions of the body surface and u, $v \in [0,1]$; D_{ij} is the control point of the body surface, S_{ij} is the control point of the distributed source at a given moment; w_{ij} is the weight in relation to the control points; m, n are the numbers of the control points in the u, v directions, respectively; $N_{i,k}(u)$, $N_{j,l}(v)$ are the B-spline basis functions, k, l are the degrees of B-spline basis functions, which is chosen as 3 in the present study, providing a C^2 continuous representation of the body surface.

3.1 Space discretization

The surfaces of Ship 1 and Ship 2 are discretized into $m(S_1)\times n(S_1)$ and $m(S_2)\times n(S_2)$ panels, respectively. $m(S_1)$ and $m(S_2)$ denote the panel numbers in the transverse direction, while $n(S_1)$, $n(S_2)$, $n(B_1)$ and $n(B_2)$ denote the panel numbers in the longitudinal direction. The total number of the collocation points is $\left(m(S_1)+1\right)\times\left(n(S_1)+1\right)+\left(m(S_2)+1\right)\times\left(n(S_2)+1\right)$

The source point $Q(u, v)$ is distributed on the Gauss points of each panel on the boundary surfaces. In the present study, 2×2 Gauss points are sufficient, as shown in Fig. 2.

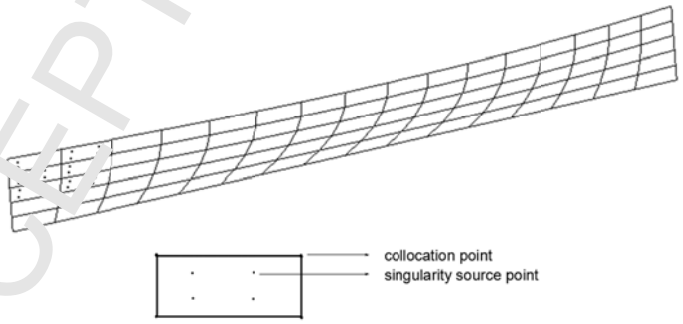

Fig. 2. Sketch of source distribution on the hull surface

Substituting Eq. (12) into Eq. (7), it follows:

$$\frac{2\pi\sum_{i=0}^{m}\sum_{j=0}^{n}w_{ij}S_{ij}N_{i,3}(u_0)N_{j,3}(v_0)}{\sum_{i=0}^{m}\sum_{j=0}^{n}w_{ij}N_{i,3}(u_0)N_{j,3}(v_0)}+$$

$$\frac{\sum_{i=0}^{m}\sum_{j=0}^{n}S_{ij}\int_0^1\int_0^1 N_{i,3}(u)N_{j,3}(v)\sum_{a=-\infty}^{\infty}\nabla\left\{\frac{1}{r_a\left[P(u_0,v_0),Q(u,v)\right]}+\frac{1}{\overline{r}_a\left[P(u_0,v_0),Q(u,v)\right]}\right\}\cdot\vec{n}(P(u_0,v_0))R\,dudv}{\sum_{i=0}^{m}\sum_{j=0}^{n}w_{ij}N_{i,3}(u)N_{j,3}(v)} \tag{13}$$

$$=\begin{cases}U_1 n_1\left(P(u_0,v_0)\right), & P\in S_1\\ U_2 n_1\left(P(u_0,v_0)\right), & P\in S_2\end{cases}$$

where $R=\sqrt{E(u_0,v_0)\cdot H(u_0,v_0)-F^2(u_0,v_0)}$ and $E=P_u\cdot P_u$, $F=P_u\cdot P_v$, $H=P_v\cdot P_v$.

The B-spline basis function $N_{i,3}(u)$ is a recursion function, and takes the form as below.

$$\begin{cases}N_{i,0}(u)=\begin{cases}1, & \text{if } u_i\le u<u_{i+1}\\ 0, & \text{otherwise}\end{cases}\\ N_{i,3}(u)=\dfrac{u-u_i}{u_{i+3}-u_i}N_{i,2}(u)+\dfrac{u_{i+4}-u}{u_{i+4}-u_{i+1}}N_{i+1,2}(u)\\ \text{stipulate}\quad \dfrac{0}{0}=0\end{cases} \tag{14}$$

The discrete form of the Fredholm integral equation of second kind is satisfied on the collocation points $P(u_0, v_0)$.

For the collocation $P(u_0, v_0)$ on the surface of Ship 1, the space discrete equation takes the form as follows:

$$\begin{aligned}&2\pi\sum_{i=0}^{m(S_1)}\sum_{j=0}^{n(S_1)}S_{ij}^{S_1}N_{i,3}(u_0)N_{j,3}(v_0)+\\ &\sum_{i=0}^{m(S_1)}\sum_{j=0}^{n(S_1)}S_{ij}^{S_1}\int_0^1\int_0^1 N_{i,3}(u)N_{j,3}(v)\nabla\left\{\frac{1}{r\left[P(u_0,v_0),Q(u,v)\right]}+\frac{1}{\overline{r}\left[P(u_0,v_0),Q(u,v)\right]}\right\}\cdot\vec{n}(P(u_0,v_0))R\,dudv+\\ &\sum_{i=0}^{m(S_2)}\sum_{j=0}^{n(S_2)}S_{ij}^{S_2}\int_0^1\int_0^1 N_{i,3}(u)N_{j,3}(v)\nabla\left\{\frac{1}{r\left[P(u_0,v_0),Q(u,v)\right]}+\frac{1}{\overline{r}\left[P(u_0,v_0),Q(u,v)\right]}\right\}\cdot\vec{n}(P(u_0,v_0))R\,dudv+\\ &\sum_{i=0}^{m(B_1)}\sum_{j=0}^{n(B_1)}S_{ij}^{B_1}\int_0^1\int_0^1 N_{i,3}(u)N_{j,3}(v)\nabla\left\{\frac{1}{r\left[P(u_0,v_0),Q(u,v)\right]}+\frac{1}{\overline{r}\left[P(u_0,v_0),Q(u,v)\right]}\right\}\cdot\vec{n}(P(u_0,v_0))R\,dudv+\\ &\sum_{i=0}^{m(B_2)}\sum_{j=0}^{n(B_2)}S_{ij}^{B_2}\int_0^1\int_0^1 N_{i,3}(u)N_{j,3}(v)\nabla\left\{\frac{1}{r\left[P(u_0,v_0),Q(u,v)\right]}+\frac{1}{\overline{r}\left[P(u_0,v_0),Q(u,v)\right]}\right\}\cdot\vec{n}(P(u_0,v_0))R\,dudv\\ &=U_1 n_1\left(P(u_0,v_0)\right)\end{aligned} \tag{15}$$

For the collocation $P(u_0, v_0)$ on the surface of Ship 2, the space discrete equation takes the form as follows:

$$
\begin{aligned}
&2\pi\sum_{i=0}^{m(S_2)}\sum_{j=0}^{n(S_2)} S_{ij}^{S_2} N_{i,3}(u_0) N_{j,3}(v_0) + \\
&\sum_{i=0}^{m(S_1)}\sum_{j=0}^{n(S_1)} S_{ij}^{S_1}\int_0^1\int_0^1 N_{i,3}(u) N_{j,3}(v)\nabla\left\{\frac{1}{r\left[P(u_0,v_0),Q(u,v)\right]}+\frac{1}{\bar{r}\left[P(u_0,v_0),Q(u,v)\right]}\right\}\cdot\vec{n}\left(P(u_0,v_0)\right)R\,dudv + \\
&\sum_{i=0}^{m(S_2)}\sum_{j=0}^{n(S_2)} S_{ij}^{S_2}\int_0^1\int_0^1 N_{i,3}(u) N_{j,3}(v)\nabla\left\{\frac{1}{r\left[P(u_0,v_0),Q(u,v)\right]}+\frac{1}{\bar{r}\left[P(u_0,v_0),Q(u,v)\right]}\right\}\vec{n}\left(P(u_0,v_0)\right)R\,dudv + \\
&\sum_{i=0}^{m(B_1)}\sum_{j=0}^{n(B_1)} S_{ij}^{B_1}\int_0^1\int_0^1 N_{i,3}(u) N_{j,3}(v)\nabla\left\{\frac{1}{r\left[P(u_0,v_0),Q(u,v)\right]}+\frac{1}{\bar{r}\left[P(u_0,v_0),Q(u,v)\right]}\right\}\vec{n}\left(P(u_0,v_0)\right)R\,dudv + \\
&\sum_{i=0}^{m(B_2)}\sum_{j=0}^{n(B_2)} S_{ij}^{B_2}\int_0^1\int_0^1 N_{i,3}(u) N_{j,3}(v)\nabla\left\{\frac{1}{r\left[P(u_0,v_0),Q(u,v)\right]}+\frac{1}{\bar{r}\left[P(u_0,v_0),Q(u,v)\right]}\right\}\cdot\vec{n}\left(P(u_0,v_0)\right)R\,dudv \\
&= U_2 n_1\left(P(u_0,v_0)\right)
\end{aligned}
\tag{16}
$$

Satisfying Eqs. (16) and (17) on each of the collocation points, and assembling them into a matrix form, it follows:

$$
\begin{bmatrix} A^{S_1S_1} & A^{S_1S_2} \\ A^{S_2S_1} & A^{S_2S_2} \end{bmatrix}\begin{bmatrix} S_I^{S_1} \\ S_I^{S_2} \end{bmatrix} = \begin{bmatrix} b_I^{S_1} \\ b_I^{S_2} \end{bmatrix} \tag{17}
$$

where

$$
A^{S_1S_1} = 2\pi\sum_{i=0}^{m(S_1)}\sum_{j=0}^{n(S_1)} N_{i,3}(u_I) N_{j,3}(v_J) + \sum_{i=0}^{m(S_1)}\sum_{j=0}^{n(S_1)}\int_0^1\int_0^1 N_{i,3}(u) N_{j,3}(v)\nabla\left\{\frac{1}{r\left[P(u_I,v_J),Q(u,v)\right]}+\frac{1}{\bar{r}\left[P(u_I,v_J),Q(u,v)\right]}\right\}\cdot\vec{n}\left(P(u_I,v_J)\right)R\,dudv,
$$
$$
I = 0,1,...,m(S_1), J = 0,1,...,n(S_1)
$$

$$
A^{S_1S_2} = \sum_{i=0}^{m(S_1)}\sum_{j=0}^{n(S_1)}\int_0^1\int_0^1 N_{i,3}(u) N_{j,3}(v)\nabla\left\{\frac{1}{r\left[P(u_I,v_J),Q(u,v)\right]}+\frac{1}{\bar{r}\left[P(u_I,v_J),Q(u,v)\right]}\right\}\cdot\vec{n}\left(P(u_I,v_J)\right)R\,dudv,
$$
$$
I = 0,1,...,m(S_1), J = 0,1,...,n(S_1)
$$

$$
A^{S_2S_1} = \sum_{i=0}^{m(S_2)}\sum_{j=0}^{n(S_2)}\int_0^1\int_0^1 N_{i,3}(u) N_{j,3}(v)\nabla\left\{\frac{1}{r\left[P(u_I,v_J),Q(u,v)\right]}+\frac{1}{\bar{r}\left[P(u_I,v_J),Q(u,v)\right]}\right\}\cdot\vec{n}\left(P(u_I,v_J)\right)R\,dudv,
$$
$$
I = 0,1,...,m(S_2), J = 0,1,...,n(S_2)
$$

$$
A^{S_2S_2} = 2\pi\sum_{i=0}^{m(S_2)}\sum_{j=0}^{n(S_2)} N_{i,3}(u_I) N_{j,3}(v_J) + \sum_{i=0}^{m(S_2)}\sum_{j=0}^{n(S_2)}\int_0^1\int_0^1 N_{i,3}(u) N_{j,3}(v)\nabla\left\{\frac{1}{r\left[P(u_I,v_J),Q(u,v)\right]}+\frac{1}{\bar{r}\left[P(u_I,v_J),Q(u,v)\right]}\right\}\cdot\vec{n}\left(P(u_I,v_J)\right)R\,dudv,
$$
$$
I = 0,1,...,m(S_2), J = 0,1,...,n(S_2)
$$

$$
S_I^{S_1} = S_{ij}^{S_1}(i = 0,1,...,m(S_1), j = 0,1,...,n(S_1))
$$

$$
S_I^{S_2} = S_{ij}^{S_2}(i = 0,1,...,m(S_2), j = 0,1,...,n(S_2))
$$

$$
b_I^{S_1} = U_1 n_1\left(P(u_i,v_j)\right)(i = 0,1,...,m(S_1), j = 0,1,...,n(S_1), I = i + j\times(n(S_1)+1))
$$

$$
b_I^{S_2} = U_2 n_1\left(P(u_i,v_j)\right)(i = 0,1,...,m(S_2), j = 0,1,...,n(S_2), I = i + j\times(n(S_2)+1))
$$

By solving the discretized Eq. (17), the control points S_{ij} for source density can be determined; then by substituting S_{ij} into Eq. (12), the source density on the body surfaces is obtained, and from Equation (5), the velocity potential at arbitrary point in the fluid field can be determined. Finally, the hydrodynamic interaction forces can be calculated according to Eq. (10).

3.2 Time discretization

To update the velocity potential on the ship surfaces during the unsteady relative motions between the two ships and to mimic the change of positions for each ship, a time-stepping method is used (Xu et al. [24]). At each time step, the longitudinal position of Ship 1 and Ship 2 are updated as defined by Eqs. (18) and (19), respectively. The velocity potential ϕ is updated from Eq. (5), and the pressure is determined by Eq. (20) at each time step:

$$U_1 = \frac{x_1(t+\Delta t) - x_1(t)}{\Delta t} \tag{18}$$

$$U_2 = \frac{x_2(t+\Delta t) - x_2(t)}{\Delta t} \tag{19}$$

$$p = -\rho\left(\frac{\phi(t+\Delta t) - \phi(t)}{\Delta t} - U_i\phi_x + \frac{1}{2}\nabla\phi\cdot\nabla\phi\right) \tag{20}$$

4. Ship geometries

There were four types of ships measured in Vantorre et al. [2], defined as ship C, D, E and H, respectively. The main parameters of the real ships and ship models are given in Table 1 and Table 2, respectively. Taking ships E and H as present numerical study objects, the hydrodynamic interaction forces on these two hulls are calculated. According to Vantorre et al. [2], Ship E was selected as own ship (indicated by subscript '$_O$'), while Ship H used as target ship (indicated by subscript '$_T$'). The speeds of own ship and target ship are denoted as U_O and U_T, the breadth of own ship and target ship are denoted as B_O and B_T, the draft of own ship and target ship are denoted as T_O and T_T, respectively.

Table 1 Main parameters of the ship models (Scale ratio is 1:75)

Ship	C			D			E			H	
Ship type	bulk carrier			container carrier			large tanker			small tanker	
Ship length L (m)	3.984			3.864			3.824			2.210	
Breadth B (m)	0.504			0.550			0.624			0.296	
Draft T (m)	0.155	0.18	0.20	0.155	0.18	0.20	0.136	0.207	0.256	0.125	0.178
Block coefficient C_B (-)	0.829	0.843	0.857	0.561	0.588	0.609	0.798	0.816	0.829	0.796	0.83

Table 2 Main parameters of the real ships

Ship	C			D			E			H	
Ship type	bulk carrier			container carrier			large tanker			small tanker	
Ship length L (m)	298.8			289.8			286.8			165.8	
Breadth B (m)	37.5			41.25			46.8			22.2	
Draft T (m)	11.63	13.5	15.0	11.63	13.5	15.0	10.2	15.53	19.2	9.38	13.35
Block coefficient C_B (-)	0.829	0.843	0.857	0.561	0.588	0.609	0.798	0.816	0.829	0.796	0.83

The NURBS panels of Ship E and H are shown in Fig. 3.

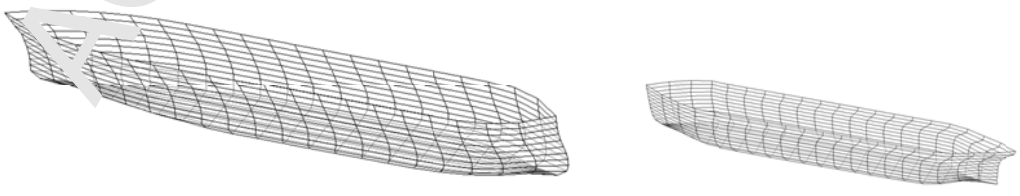

(a) (b)

Fig. 3. Ship surfaces represented by NURBS: (a) Ship E; (b) Ship H

5. Numerical results and discussions

The numerical results of hydrodynamic forces and yaw moment are normalized as:

$$CF_{ix}=\frac{F_{ix}}{\frac{1}{2}\rho L_i T_i (U_O^2-U_O U_T+U_T^2)},\quad CF_{iy}=\frac{F_{iy}}{\frac{1}{2}\rho L_i T_i (U_O^2-U_O U_T+U_T^2)},\quad C_{in}=\frac{M_{in}}{\frac{1}{2}\rho L_i^2 T_i (U_O^2-U_O U_T+U_T^2)} \tag{21}$$

where i corresponds to own ship or target ship. It should be noted that only the hydrodynamic interaction forces and moments acting on own ship are investigated.

As an important parameter in ship-ship interactions the normalized longitudinal distance between the two ships, $\xi=2.0ST/(L_O+L_T)$, is used to replace time t in the time stepping method. Considering the reality that the interaction hydrodynamic forces vanish to zero when the longitudinal distance between ships is larger than two times of ship length, the calculation starts at an initial position of $\xi=-2.0$ and ends at the position of $\xi=2.0$.

5.1. Validation cases

5.1.1. Ship E meeting Ship H

According to the experimental conditions and the coordinate systems defined in Fig. 1, own ship's speed in full scale is U_O =12knots (6.1728m/s), target ship's speed is U_T = 12knots (6.1728m/s), the broadside distance between two ships y_{bb} = 11.1m = $0.237B_O$, and the water depth h = 18.63m =$1.2T_O$. Before the validation of numerical results, a convergence study should be conducted. According to the previous study in Xu and Zou [23], 30×20 panels on each hull and the time step of 0.705s are appropriate. Also, for the infinite image Green function in Eq. (6), the truncated version takes the form as Eq. (22), and the number of reflections n=6 is sufficient. The computational model of Ship E meeting Ship H is shown in Fig. 4. The predicted surge force, lateral force and yaw moment acting on own ship during meeting are shown in Fig. 5, comparing with both experimental data [7] and results from the constant panel method [16]. Obviously, the results verify that the interaction forces and moments between the two ships are notable within twice of the ship length and vanish to zero as the nominal distance becomes larger than 2.0.

$$G(x,y,z;\xi,\eta,\zeta)=\sum_{a=-n}^{n}\left(\frac{1}{r_a}+\frac{1}{\bar{r}_a}\right) \tag{22}$$

The surge forces are characterized by negative at $\xi<0$ (the peak value occurs around $\xi=-0.5$), while positive at $\xi>0$ (the peak value occurs around $\xi=0.4$). The lateral force is characterized by an initial repulsion, followed by attraction and finally repulsion force again. The peak value of repulsion occurs when $\xi\approx\pm0.8$, while the peak value of attraction occurs when $\xi\approx0$. For the yaw moment, there are four phases to be distinguished which are characterized by consecutive actions of bow repulsion, bow attraction, bow repulsion and bow attraction. The peak value of bow repulsion occurs when $\xi\approx-0.8$ and $\xi\approx0.3$, and the peak value of bow attraction occurs when $\xi\approx-0.3$ and $\xi\approx0.8$.

For the surge force, both the present results of high-order panel method and those of constant panel method agree well with the experimental measurements. For the lateral force, both methods approximately agree with, while a bit smaller than the experimental measurements at the repulsion stage. It may be mainly due to that the numerical results of the present high-order panel method and those of constant panel method are based on the potential flow theory with the assumption of inviscid flow and low speed under which the wave-making effect is ignored. According to Pinkster [33], when two ships navigating in open water with low speeds, the wave-making effect does not have remarkable influences on interaction forces and moments. Therefore, the viscosity of fluid may be the main reason causing under-predicted results. Similarly, for the yaw moment, both results agree well with the experimental measurements, while the peak values of numerical results are slightly smaller than those of experimental measurements.

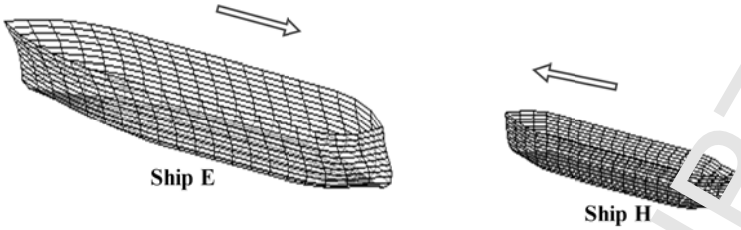

Fig. 4. Computation model of Ship E meeting Ship H

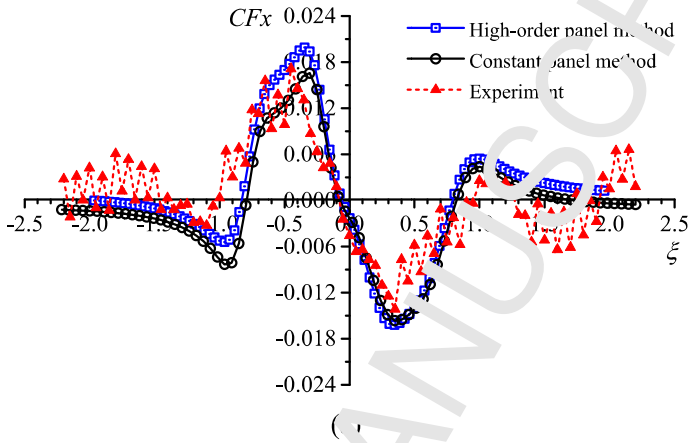

(a)

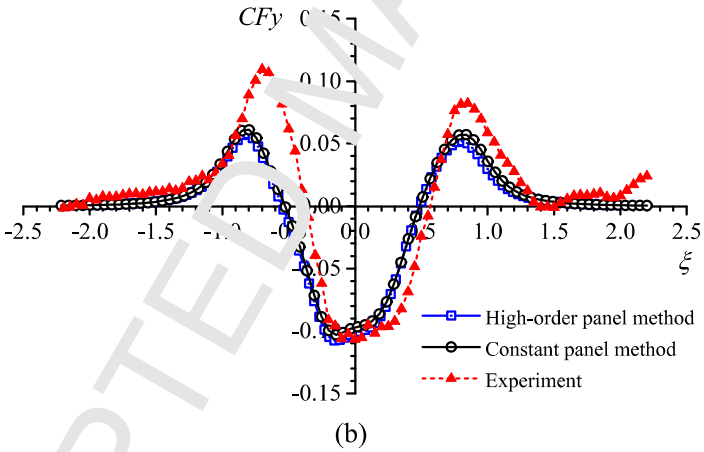

(b)

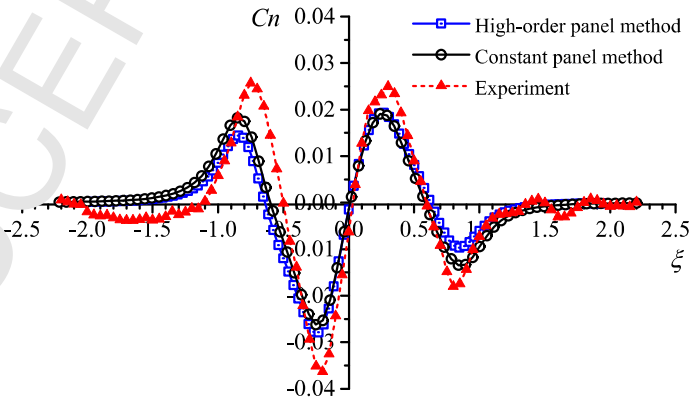

(c)

Fig. 5. Validation of surge forces, lateral forces and yaw moments acting on own ship during meeting; $h/T_O = 1.2$, $y_{bb} = 0.237B_O$, $U_O = -U_T = 6.1728$m/s

5.1.2. Ship E overtaken by Ship H

In accordance with the model test conditions, own ship's speed U_O = 8knots (4.1152m/s), target ship's speed U_T = 12knots (6.1728m/s), the broadside distance between two ships $y_{bb} = 0.27B_O$, and the water depth h = 18.63m = $1.2T_O$. Similarly, according to the previous convergence study [23], 30×20 panels on each hull and the time step of 4.229s are appropriate. Still, for the infinite image Green function truncated terms, n=6 is sufficient. The computational model of Ship E overtaken by Ship H is shown in Fig.6. The calculation data of surge force, lateral force and yaw moment acting on own ship E are compared with both experimental data [2] and results from the constant panel method [16] during overtaking, as shown in Fig. 7.

Obviously, the interaction forces and moments emerge in the longitudinal distance between two ships within twice of ship length and vanish to zero as the distance tends to be larger. Moreover, the surge force is characterized by negative at $\xi<0$ (the peak value occurs near $\xi=-0.4$), while characterized by positive at $\xi>0$ (the peak value occurs at $\xi=0.5$). The lateral forces are characterized by an initial repulsion, followed by attraction and finally repulsion again. The peak value of repulsion occurs when $\xi\approx\pm0.7$, while the peak value of attraction occurs when $\xi\approx0.2$. For the yaw moment, there are four distinguished phases. That is, two consecutive bow repulsion and bow attraction. The peak value of bow repulsion occurs when $\xi\approx-0.3$, and the peak value of bow attraction occurs when $\xi\approx0.3$.

For the surge force, both the present numerical results with high-order panel method and those with constant panel method agree well with the experimental measurements. While at the negative surge force stage, the peak values of numerical results are smaller than those of experimental measurements. For the lateral force, the numerical results of both methods approximately agree with, while a bit smaller than the experimental measurements, and the present numerical results of high-order panel method are even better. It is mainly because that both methods are based on the potential flow theory with the assumption of inviscid flow, and the numerical results are based on the assumption of low speed, and wave-making effect is ignored. According to Xu and Zou [23], viscous effect of fluid does not have remarkable influences on interaction forces during two ships overtaking at low speed in open water. Therefore, the wave-making effect is the main reason that cause the smaller numerical results. For the yaw moment, the present numerical results of high-order panel method agree with those of constant panel method almost unanimously, while the peak values of the numerical results are smaller than those of experimental measurements by almost 40% during the bow repulsion stage.

It is shown that the present high-order panel method based on NURBS is able to predict qualitatively the tendency of the interaction forces, while as the calculation is under the frame of potential flow theory, and the wave-making effect is ignored under the assumption of low ship speed, thus the present numerical results are slightly smaller than those of experimental measurements.

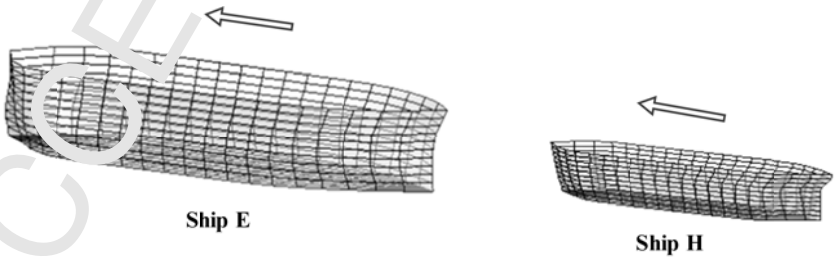

Fig. 6. Computation model of Ship E overtaken by Ship H

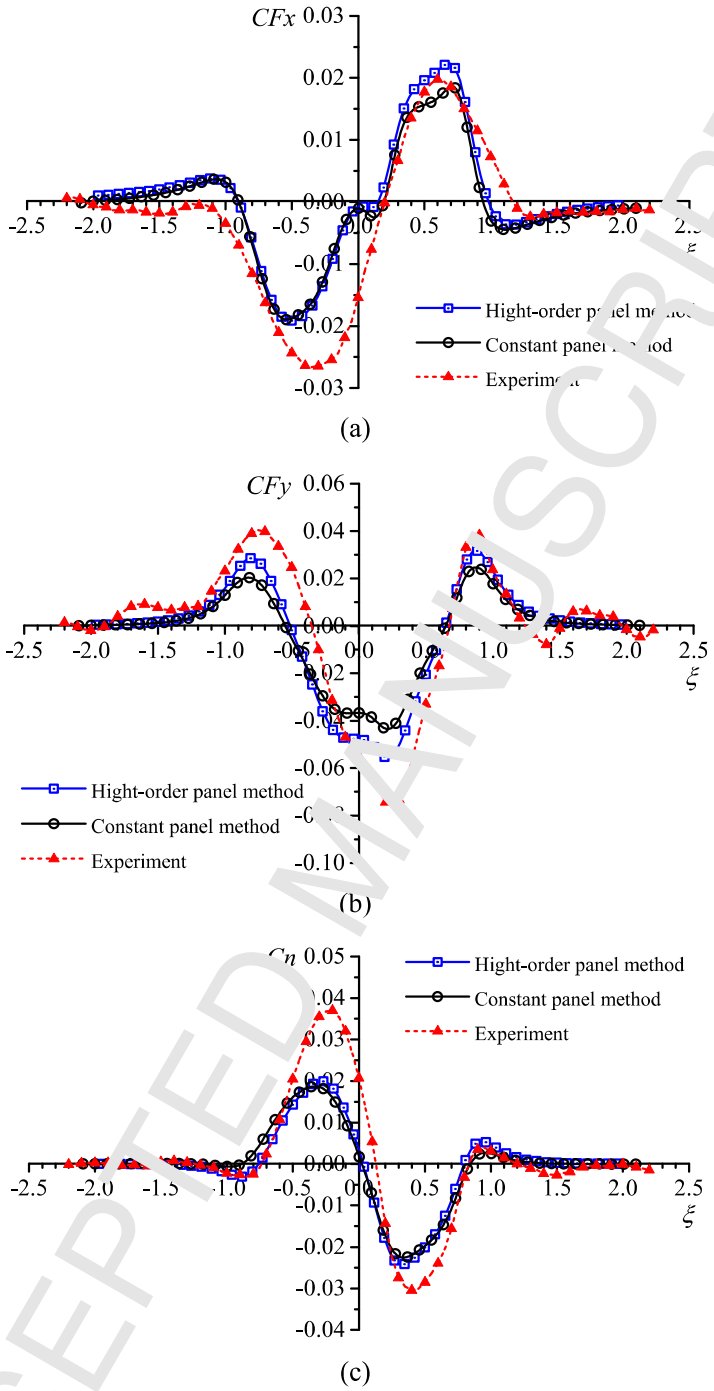

Fig. 7. Validation of surge forces, lateral forces and yaw moments acting on own ship during Ship E overtaken by ship H; $h/T_O = 1.2$, $y_{bb} = 0.237B_O$, $U_O = 4.1152$m/s, $U_T = 6.1728$m/s

5.2. Influence of water depth

5.2.1. Case of Ship E meeting Ship H

To investigate the influence of water depth on the hydrodynamic interaction forces during meeting, calculations are conducted for different water depth to draft ratios $h/T_O = 1.2$, 1.3, 1.5, 1.8 and 2.0, while the lateral distance between ships' broadsides is $y_{bb} = 0.237B_O$, own ship's speed $U_O = 12$knots (6.1728m/s), and target ship's speed $U_T = 12$knots (6.1728m/s). The surge forces, lateral forces and yaw moments acting on own ship are shown in Fig. 8.

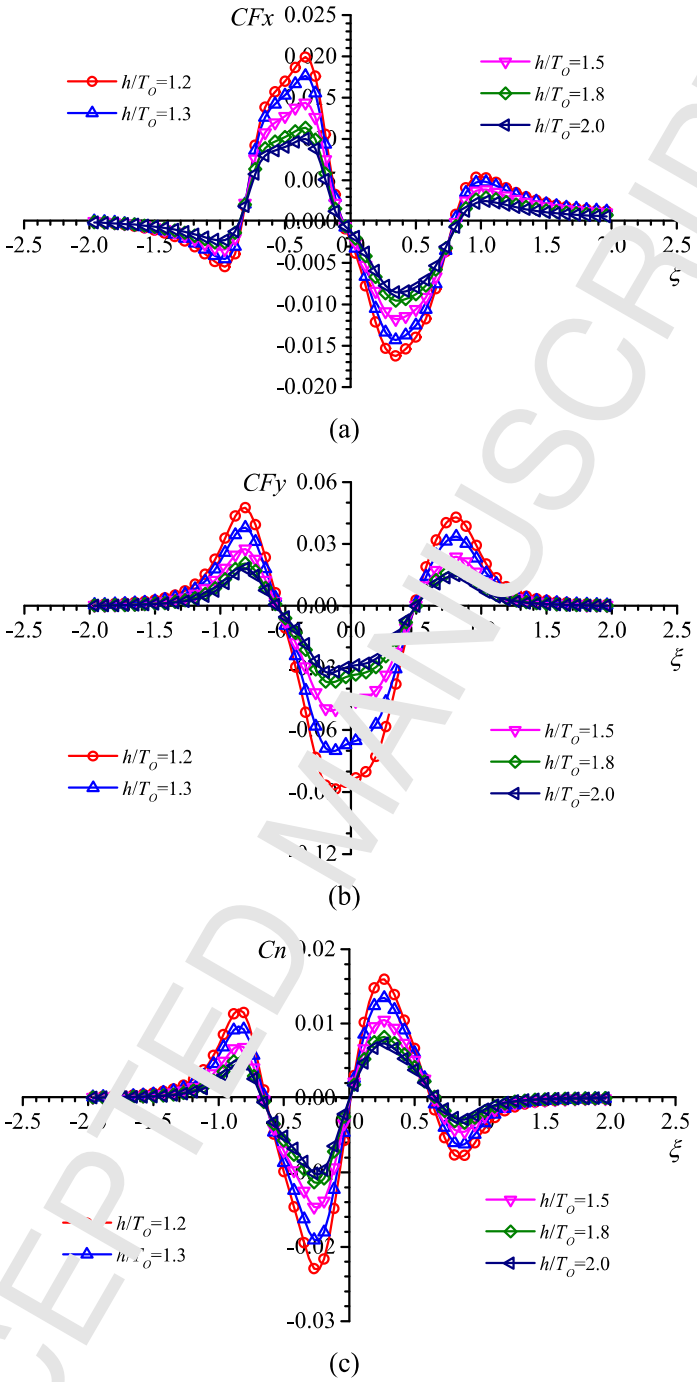

Fig. 8. Comparison of surge forces, lateral forces and yaw moments acting on own ship at different ratios of water depth to own ship's draft in meeting condition; $y_{bb} = 0.237B_O$, $U_O = -U_T = 6.1728$m/s

It can be seen that the tendency with varying ship-ship longitudinal distance is similar to previous validation case of meeting ships (see Fig. 5), while with different water depths, the magnitudes of the hydrodynamic interaction force and moment increase with the decrease of water depth, and vice versa. It's known as shallow water effect. A remarkable increase of the force and moment can be found when $h/T_O \leqq 1.5$.

5.2.2. Case of Ship E overtaken by Ship H

To investigate the influence of water depth on the hydrodynamic interaction forces during overtaking, calculations are conducted for different water depth to draft ratio h/T_O = 1.2, 1.3, 1.5, 1.8 and 2.0; while the lateral distance between ships' broadsides $y_{bb} = 0.237B_O$, own ship's speed U_O = 8 knots (4.1152m/s), and target ship's speed U_T =12knots (6.1728m/s) remain unchanged. The surge forces, lateral forces and yaw moments acting on own ship are shown in Fig. 9. The tendency against the water depth is similar to the meeting case: the magnitudes of the hydrodynamic interaction force and moment increase with the decrease of water depth, and the increase is also more notable as $h/T_O \leqq 1.5$.

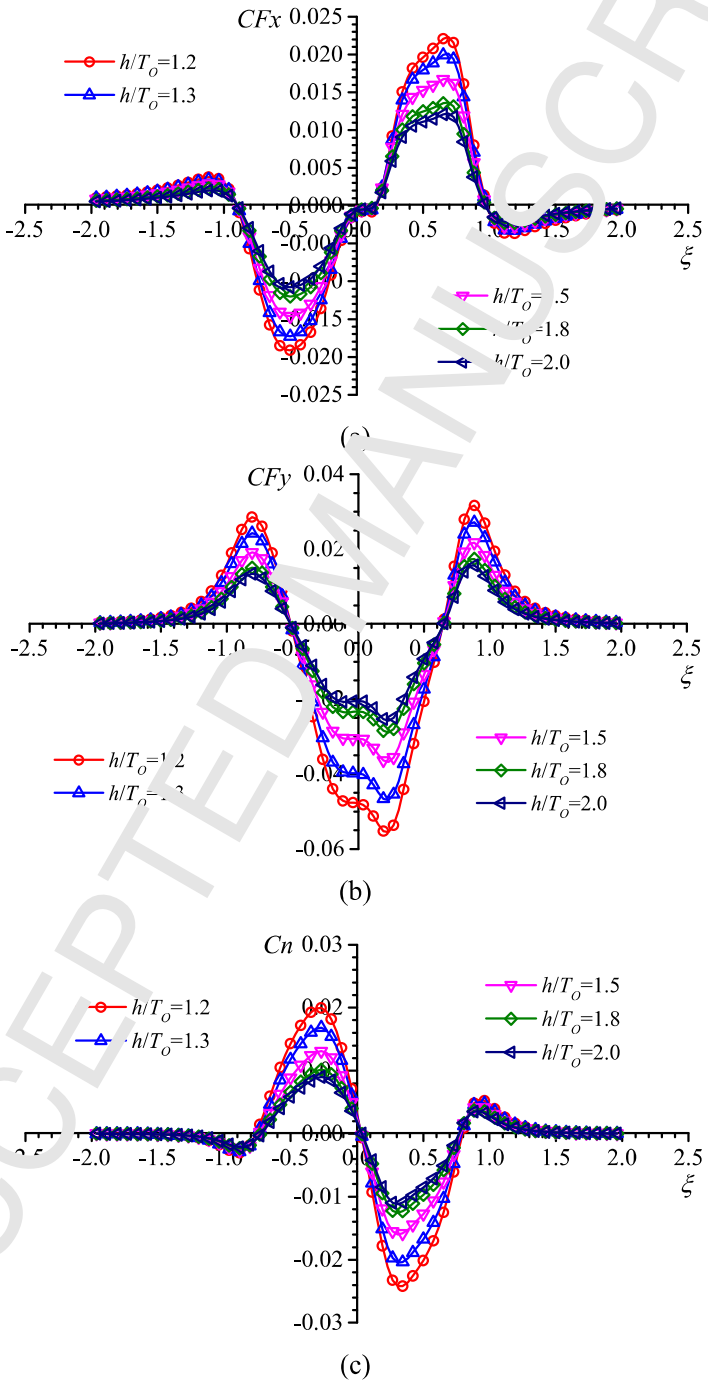

Fig.9. Comparison of surge forces, lateral forces and yaw moments acting on own ship at different ratios of water depth to own ship's draft during Ship E overtaken by Ship H;
$y_{bb} = 0.237B_O$, U_O = 4.1152m/s, U_T = 6.1728m/s

5.3. Influence of lateral distance between ships

5.3.1. Case of Ship E meeting Ship H

To investigate the influence of the lateral distance between ships during meeting, different lateral distances between ships' broadsides are simulated, including $y_{bb} = 0.25B_O$, $0.50B_O$, $1.00B_O$, $2.00B_O$, $3.00B_O$, $4.00B_O$ and $5.00B_O$, while the water depth $h/T_O = 1.2$, own ship's speed $U_O = 12$knots (6.1728m/s), and target ship's speed $U_T = 12$knots (6.1728m/s) are the same as the validation case. The surge forces, lateral forces and yaw moments acting on own ship are shown in Fig.10. The tendency is similar for different lateral distance between ships during meeting, and the magnitudes of the hydrodynamic interaction force and moment increase with the decrease of lateral distance between ships, and vice versa. It's because of the emergence of asymmetry flow, and asymmetry flow is intensified with the decrease of lateral distance. There is a clear increase of force and moment at $y_{bb} = 2.00B_O$, and when the distance is smaller, the increase is even more pronounced.

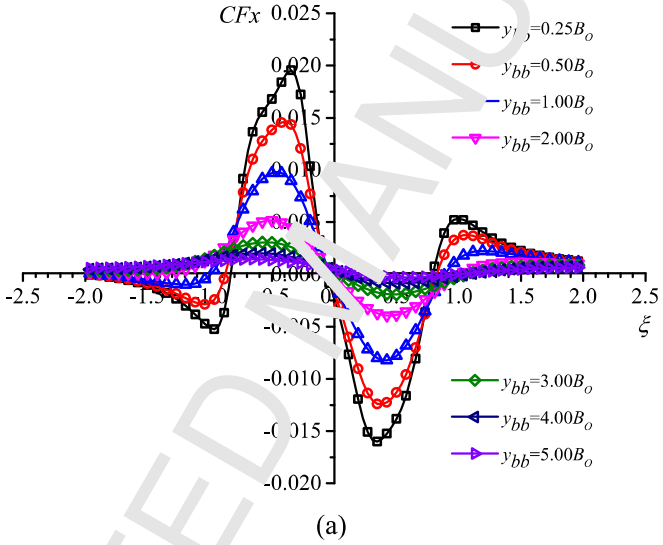

(a)

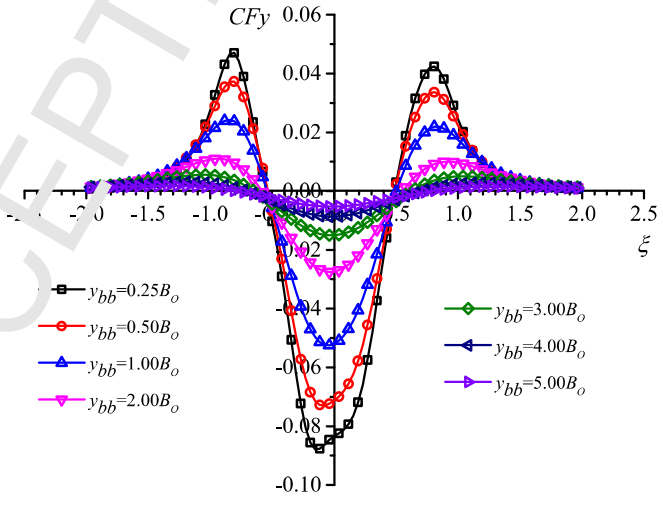

(b)

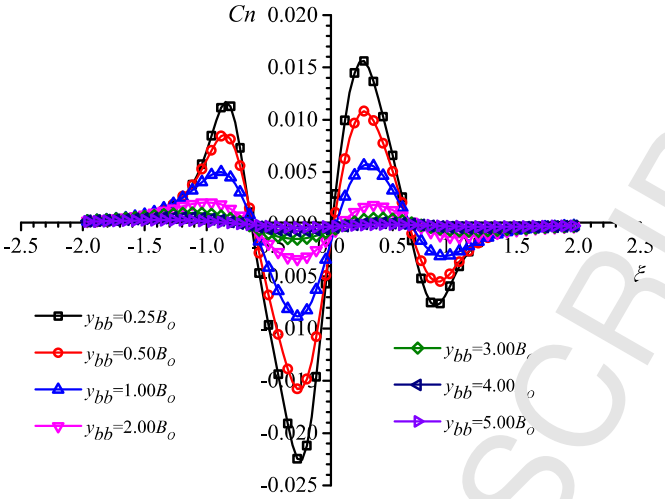

(c)

Fig.10. Comparison of surge forces, lateral forces and yaw moments acting on own ship at different lateral distances in meeting condition; h/T_O = 1.2, U_O = −U_T = 6.1728m/s

5.3.2. Case of Ship E overtaken by Ship H

Similarly, to investigate the influence of the lateral distance between ships on the hydrodynamic interaction forces during overtaking, calculations are conducted for different lateral distances between ships' broadsides with the same variations as with the meeting cases in Section 5.3.1, while the water depth h/T_O = 1.2, own ship's speed U_O = 8knots (4.1152m/s), and target ship's speed U_T = 12knots (6.1728m/s) keep the same as the validation case. The surge forces, lateral forces and yaw moments acting on own ship are shown in Fig.11. The tendency is similar to the meeting case: intense ship-ship interaction forces and moment should be noted especially when y_{bb} = 2.00B_O.

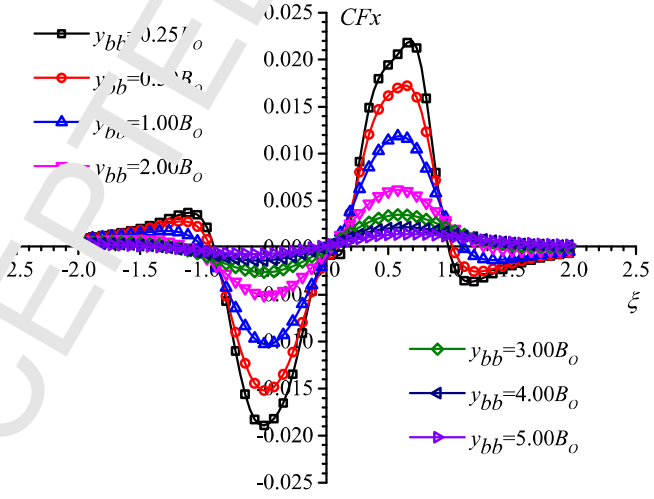

(a)

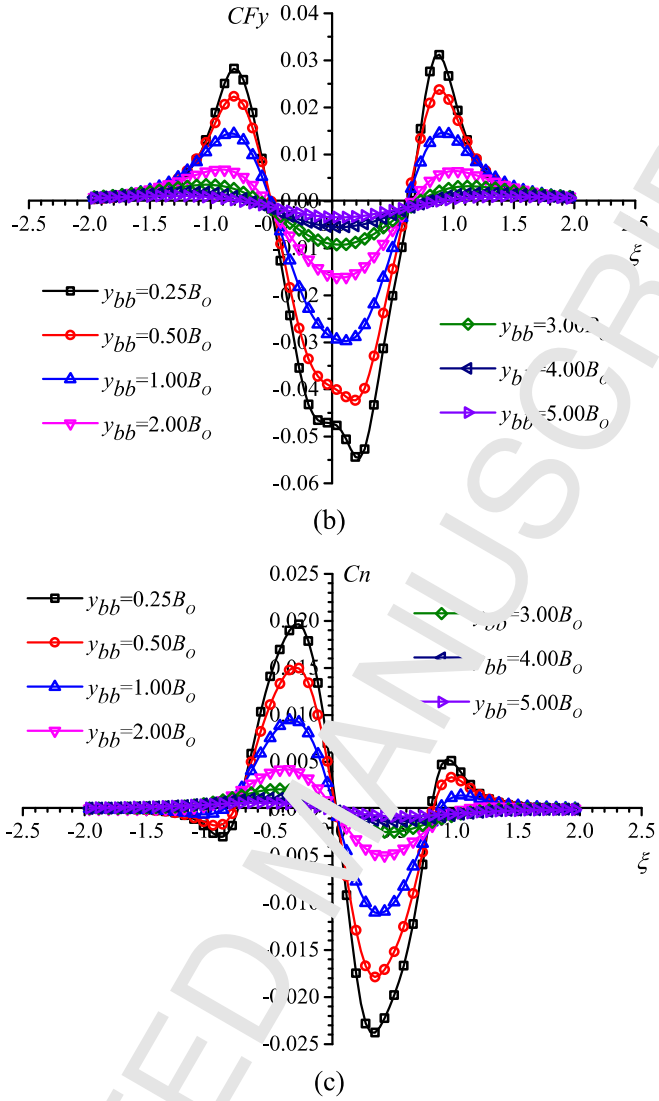

Fig. 11. Comparison of surge forces, lateral forces and yaw moments acting on own ship at different lateral distances during Ship E overtaken by Ship H; h/T_O = 1.2, U_O = 4.1152m/s, U_T = 6.1728m/s

5.4. Influence of ship speeds

5.4.1. Case of Ship E meeting Ship H

To investigate the influence of ship speed on the hydrodynamic interaction, calculations are conducted from two aspects, that is, own ship's speed and target ship's speed.

(a) Influence of own ship's speed

To investigate the influence of own ship's speed, calculations are carried out for own ship's speed U_O = 0, 4 knots (2.0576m/s), 8 knots (4.1152m/s) and 12 knots (6.1728m/s). Target ship's speed U_T = 8knots (4.1152m/s). The lateral distance between the broadsides of two ships $y_{bb} = 0.237B_O$ and the water depth h/T_O = 1.2 remain unchanged. The surge forces, lateral forces and yaw moments acting on own ship are shown in Fig. 12. The magnitudes of the hydrodynamic interaction forces and moment tend to be larger with the increase of own ship's speed, typically as $U_O \geqq$ 4knots (2.0576m/s).

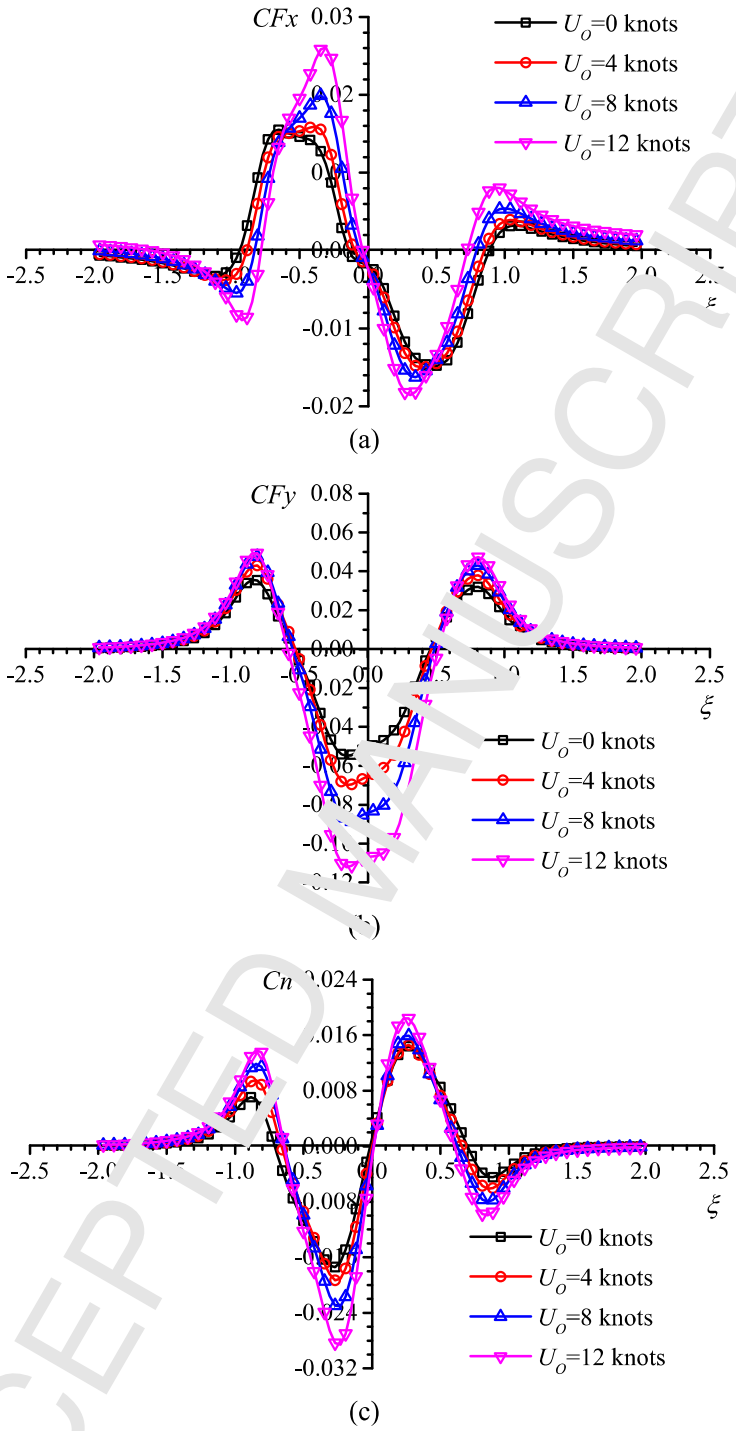

Fig. 12. Comparison of surge forces, lateral forces and yaw moments acting on own ship at different own ship's speed in meeting condition; $h/T_O = 1.2$, $y_{bb} = 0.237B_O$, $U_T = -4.1152$m/s

(b) Influence of target ship's speed

A series of target ship's speed is considered in the investigation: U_T = 0, 4knots (2.0576m/s), 8knots (4.1152m/s) and 12knots (6.1728m/s). Own ship's speed U_O = 8knots (4.1152m/s), the lateral distance between the broadsides of two ships $y_{bb} = 0.237B_O$ and the water depth $h/T_O = 1.2$ remain unchanged. The surge forces, lateral forces and yaw moments acting on own ship are shown in Fig. 13. It can be seen that the tendency against the ship position is similar to the validation case, while a pronounced increase of force or moment caused by the ship-ship interaction can be observed when there is an increase in relative speed

between own ship and target ship.

By comparing the influence of own ship's speed with that of target ship's speed, it can be seen that target ship speed plays a more remarkable role in hydrodynamic interaction forces and moment than own ship speed does.

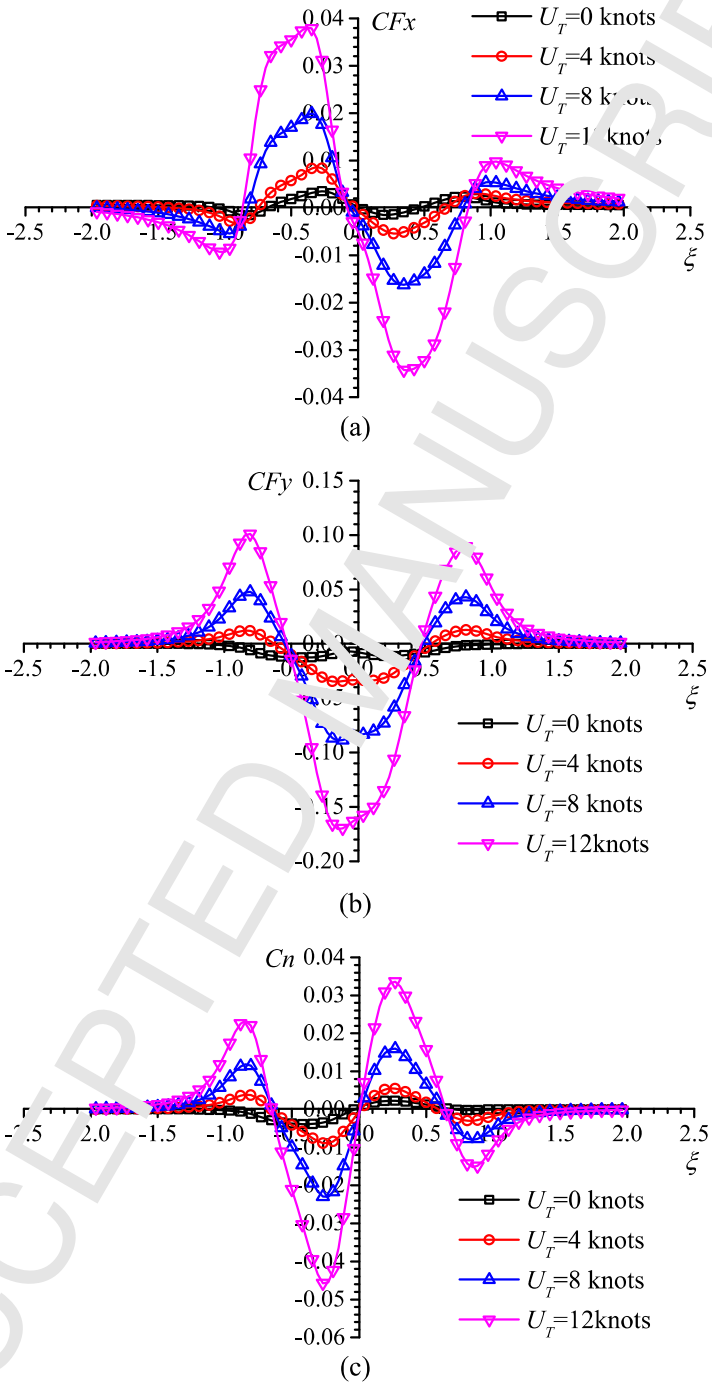

Fig. 13. Comparison of surge forces, lateral forces and yaw moments acting on own ship at different target ship's speed in meeting condition; $h/T_O = 1.2$, $y_{bb} = 0.237B_O$, $U_O = 4.1152$m/s

5.4.2. Case of Ship E overtaken by Ship H

(1) Influence of own ship's speed

To investigate the influence of own ship's speed, calculations are carried out for own ship's speed $U_O = 0$, 4knots (2.0576m/s) and 8knots (4.1152m/s). Target ship's speed $U_T = 12$knots (6.1728m/s). The lateral distance between the broadsides of two ships $y_{bb} = 0.237B_O$ and the water depth $h/T_O = 1.2$ remain unchanged. The surge force, lateral force and yaw moment acting on own ship are shown in Fig. 14. Still, comparing with the validation case in Fig. 7, a similar tendency against the ship-ship position can be found with different own ship's speed during overtaking. With the increase of own ship's speed, and the relative motion between own ship and target ship is decrease, the magnitudes of the hydrodynamic interaction force and moment decrease slightly. But the decrease of lateral force peak value a bit more obvious than that of surge force and yaw moment.

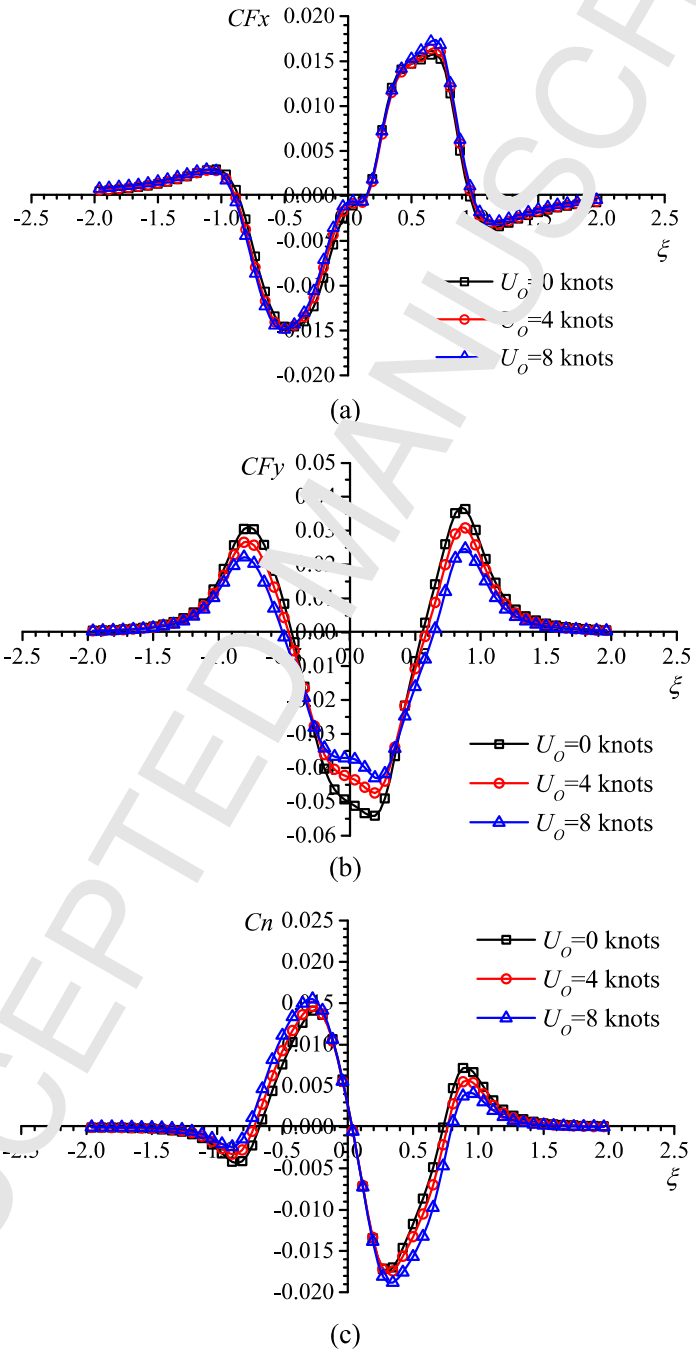

Fig. 14. Comparison of surge forces, lateral forces and yaw moments acting on own ship at different own ship's speeds during Ship E overtaken by Ship H; $h/T_O = 1.2$, $y_{bb} = 0.237B_O$, $U_T = 6.1728$m/s

(2) Influence of target ship's speed

Calculations are carried out for target ship's speed U_T = 6knots (3.0864m/s), 8knots (4.1152m/s) and 12knots (6.1728m/s). Own ship's speed U_O = 4knots (2.0576m/s). The lateral distance between the broadsides of two ships $y_{bb} = 0.237B_O$ and the water depth $h/T_O = 1.2$ remain the same. The surge forces, lateral forces and yaw moments acting on own ship are shown in Fig. 15.

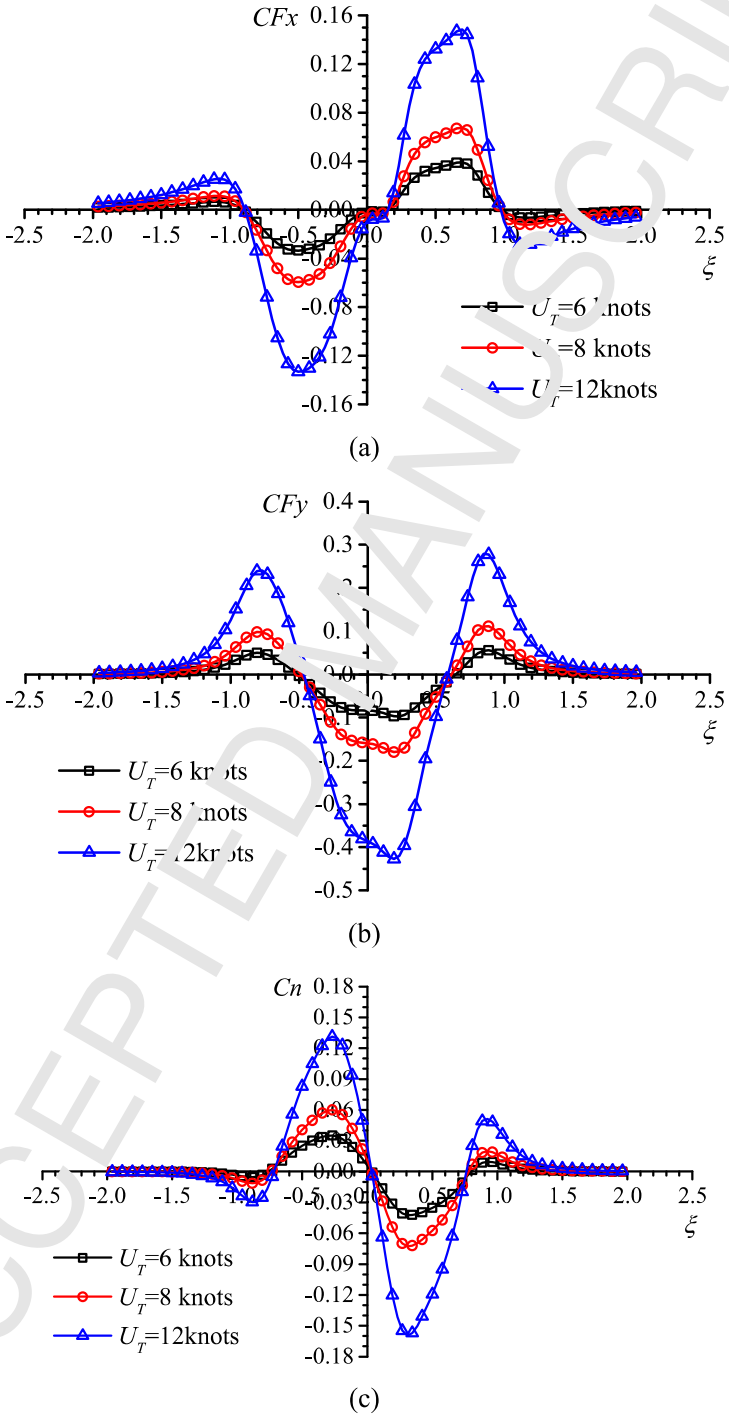

Fig. 15. Comparison of surge forces, lateral forces and yaw moments acting on own ship at different target ship's speeds during Ship E overtaken by Ship H; $h/T_O = 1.2$, $y_{bb} = 0.237B_O$, $U_O = 2.0576$m/s

By comparing the influence of own ship's speed with that of target ship's speed, it can be seen that in the

overtaking case, the variation of target ship's speed also plays a more remarkable role in hydrodynamic forces and moment acting on own ship than own ship's speed does. For both Figs. 14 and 15, this phenomenon is reasonable as during the overtaking target ship has larger speed than own ship, thus a more remarkable influence of target ship is expected.

6. Concluding remarks

The ship-ship interactions in meeting and overtaking conditions have been numerically studied by using a high-order panel method based on NURBS, and the hydrodynamic forces and moments on own ship are predicted. The boundary integral equation is solved at each time step. Under the assumption of low ship speed, the effect of free surface elevation is ignored. Comparisons with experimental measurements show that the present method is effective.

The influences of finite water depth, lateral distance between ships' broadsides on interaction forces and moments are analyzed in detail. It is found that the tendencies of the interaction forces and moments against ship-ship longitudinal distance are qualitatively similar at different water depths and lateral distances between ships, but some notable increases of interaction force and moment can be observed when the water depth or ship-ship distance is reduced, from which the limiting water depth and ship-ship distance indicating intense ship-ship interactions can be identified.

The influences of own ship's speed and target ship's speed are also investigated and shown to be noticeable. By comparing the influence of own ship's speed with that of target ship's speed, it can be found that the speed of target ship plays a more remarkable role in hydrodynamic forces and moment acting on own ship than own ship's speed does, both in meeting and overtaking conditions.

The present high-order panel method is able to predict qualitatively the tendency of the interaction forces between real ship forms. The further study will focus on extending this method to investigate the ship-ship interaction problems taking the linear boundary conditions on the free surface and viscous corrections of fluid into consideration.

Acknowledgements

This work was supported by the National Natural Science Foundation of China (grant number: 51309152).

References

[1] Remery, G.F.M., Mooring forces induced by passing ships, Paper No. 2066, Proceedings of the 6th Offshore Technology Conference (OTC), Houston, Texas, 1974.
[2] Vantorre, M., Verzhbitskaya, E., Laforce, E., Model test based formulations of ship-ship interaction forces, Ship Technology Research, 2002, 49: 124-139.
[3] Lataire, E., Vantorre, M., Delefortrie, G., Captive model testing for ship-to-ship operations, Proceedings of the International Conference on Marine Simulation and Ship Maneuverability, MARSIM'09, Panama City, Panama, 2009.
[4] Pettersen, B., Berg, T.E., Eloot, K., et al. 2nd International Conference on Ship Manoeuvring in Shallow and Confined Water: Ship to Ship Interaction: Conference proceedings, Royal Institution of Naval Architects, 2011.
[5] Tuck, E.O., Newman, J.N., Hydrodynamic interactions between ships, Proceedings of the 10th Symposium on Naval Hydrodynamics, Cambridge, Mass., USA, 1974: 35-70.
[6] Yeung, R.W., On the interactions of slender ships in shallow water, Journal of Fluid Mechanics, 1978, 85(Part 1): 143-159.
[7] Wang, Q.X., An analytical solution for two slender bodies of revolution translating in very close proximity, Journal of Fluid Mechanics. 2007, 582: 223-251.
[8] Hess, J.L., Smith, A.M.O., Calculation of non-lifting potential flow about arbitrary three-dimensional bodies, Journal of Ship Research, 1964, 8(2): 22-44.
[9] Korsmeyer, F.T., Lee, C.H., Newman J.N., Computation of ship interaction forces in restricted waters, Journal of Ship Research, 1993, 37(4): 298-306.

[10] Newman, J.N., The Green function for potential flow in a rectangular channel, Journal of Engineering Mathematics, 1992, 26: 51-59.
[11] Zhang, X.D., Wu, X.H., Study of hydrodynamic forces of ships in narrow waterway, Journal of Hydrodynamics, 2003, 15(4): 113-117.
[12] Yasukawa, H., Kawamura, S., Tanaka, S., Sano, M., Evaluation of ship-bank and ship-ship interaction forces using a 3D panel method, Proceedings of the International Conference on Ship Maneuvering in Shallow and Confined Water: Bank Effects, Antwerp, Belgium, 2009, pp. 12[illegible]-13[illegible].
[13] Sutulo, S., Guedes Soares, C., Otzen, J.F., Validation of potential-flow estimation of interaction forces acting upon ship hulls in parallel motion, Journal of Ship Research, 2012, 56(3): 129-145.
[14] Sutulo, S., Guedes Soares, C., Parametric study of a modified panel method in application to the ship-to-ship hydrodynamic interaction, Proceedings of the 4th International Conference on Ship Manoeuvring in Shallow and Confined Water, Hamburg, Germany, 2016, pp. 177-185.
[15] Zhou, X.Q., Sutulo, S., Guedes Soares, C., Computation of ship hydrodynamic interaction forces in restricted waters using potential theory, Journal of Marine Science and Application, 2012 (11): 265-275.
[16] Zhou, X.Q., Sutulo, S., Guedes Soares, C., Computation of ship-to-ship interaction forces by a three-dimensional potential-flow panel method in finite water depth, Journal of Offshore Mechanics and Arctic Engineering, 2014, 136(4), 041301.
[17] Zhou, X.Q., Sutulo, S., Guedes Soares, C., A paving algorithm for dynamic generation of quadrilateral meshes for online numerical simulations of ship manoeuvring in shallow water, Ocean Engineering, 2016, 122: 10-21.
[18] Yuan, Z.M., Incecik, A., Dai, S., et al., Hydrodynamic interactions between two ships travelling or stationary in shallow waters, Ocean Engineering. 2015, 108: 620-635.
[19] Yuan, Z.M., He, S., Kellett, P., et al., Ship-to-ship interaction during overtaking operation in shallow water, Journal of Ship Research, 2015, 59(3): 172-187.
[20] Zhang, X.T., Teng, B., Liu, Z.Y., Computation of hydrodynamic interaction forces between ships based on B-splines, Journal of Hydrodynamics, 2003, 15(2): 83-88.
[21] Xu, H.F., Zou, Z.J., Zou, L., Liu, X.Y., Unsteady hydrodynamic interaction between two cylindroids in shallow water based on high-order panel method, Engineering Analysis with Boundary Elements, 2016, 70: 134-146.
[22] Xu, H.F., Zou, Z.J., Liu, X.Y., Prediction of ship-ship interaction forces in shallow water using a high-order panel method, Journal of Ship Mechanics, 2016, 20(12): 1535-1546.
[23] Xu, H.F., Zou, Z.J., Prediction of hydrodynamic forces on a moored ship induced by a passing ship in shallow water using a high-order panel method, Journal of Shanghai Jiaotong University (Science), 2016, 21(2): 129-135.
[24] Xu, H.F., Zou, Z.J., Wu, S.W., Liu, X.Y., Zou, L., Bank effects on ship-ship hydrodynamic interaction in shallow water based on high order panel method, Ships and Offshore Structures, 2017, 12(6): 843-861.
[25] Chen, H.C., Lin, W.M., Hwang, W.Y., Validation and application of chimera RANS method for ship-ship interactions in shallow water and restricted waterway, Proceedings of the 24th Symposium on Naval Hydrodynamics, Fukuoka, Japan, 2002.
[26] Zhang, C.X., Zou, Z.J., Numerical investigation on ship-ship hydrodynamic interaction in restricted waters, Proceedings of the 2nd International Conference on Ship Maneuvering in Shallow and Confined Water: Ship-to-Ship Interaction, Trondheim, Norway, 2011, pp. 407-412.
[27] Sadat-Hosseini, H., Wu, P.C., Toda, Y., Carrica, P., Stern, F., URANS studies of ship-ship interaction in shallow water, Proceedings of the 2nd International Conference on Ship Maneuvering in Shallow and Confined Water: Ship-to-Ship Interaction, Trondheim, Norway, 2011, pp. 299-308.
[28] Zou, L., Larsson, L., Investigation of ship-to-ship interaction during lightering operations in shallow waters using a RANS solver, Proceedings of the International Conference on Marine Simulation and Ship Maneuverability, MARSIM 2012, Singapore, 2012.
[29] Zou, L., Larsson, L., Numerical predictions of ship-to-ship interaction in shallow water, Ocean Engineering, 2013, 72: 386-402.
[30] Meng, Q., Wan, D., Chen, G. Numerical simulation of ship-ship interactions in shallow water, Proceedings of the 26th International Ocean and Polar Engineering Conference, Rhodes, Greece, 2016, pp. 751-756.
[31] Wang, H.Z., Zou, Z.J., Numerical study on hydrodynamic interaction between a berthed ship and a

ship passing through a lock, Ocean Engineering, 2014, 88: 409-425.
[32] Kok, Z., Jin, Y., Chai, S., Denehy, S., Duffy, J., URANS prediction of berthed ship-passing ship interactions, Proceedings of the 36th International Conference on Ocean, Offshore and Arctic Engineering, Trondheim, Norway, 2017.
[33] Pinkster, J.A., The influence of a free surface on passing ship effects, International Shipbuilding Progress. 2004, 51(4): 313-338.

Highlights

- Ship-ship interaction in shallow water is investigated by a high-order panel method;
- Interaction hydrodynamic forces during meeting and overtaking are predicted;
- The method is validated by comparing the numerical results with experimental data,
- Computations are conducted at different water depth, ship-ship distance and ship speed;
- The influences of water depth, ship-ship distance and ship speed are demonstrated.